Microscopic height measurements on moving objects with digital holography

Annelie Schiller*, Tobias Beckmann, Markus Fratz, Alexander Bertz, Daniel Carl
Fraunhofer Institute for Physical Measurement Techniques IPM,
Georges-Köhler-Allee 301, 79110 Freiburg, Germany

ABSTRACT

Using digital holography in camera-based interferometers, 3D surface topography can be measured extremely quickly and with sub-wavelength precision. Using spatial phase-shifting, a single camera image is sufficient to reconstruct complex-valued wavefronts for multiple wavelengths. Recently, measurements on moving objects were demonstrated using setups with 1× magnification. Increasing the lateral resolution by implementing larger magnification in a microscopic setup would open up new application fields, but the larger numerical apertures (NA) of microscope objectives make the acquisition even more sensitive to motion. In this work, we show the first microscopic setup, measuring objects moving at several mm/s using two-wavelength holography. Despite the large NA of 0.42 of the 10×-objective in our setup, measurements can be acquired at 75 mm/s and beyond. Using two lasers emitting slightly different wavelengths (637.76 nm and 632.87 nm), a maximum height difference of 41.3 µm can be detected unambiguously. One single image covers a line-shaped measurement area of 3.7 mm × 0.2 mm with a lateral pixel pitch of 0.47 µm. In order to inspect larger objects, single frames can be stitched together, permitting an infinite measurement area in the direction of motion. Gap-free stitched measurements are limited to 75 mm/s due to the framerate of the camera. Measurements of the groove depth averaged over several pixels on a groove standard show a repeatability exceeding 10 nm at 35 mm/s and 20 nm at 75 mm/s.

Keywords: Digital Holography, Multiwavelength Interferometry, Interferometry in Motion, Holographic Microscopy

1. INTRODUCTION

Interferometers are very sensitive to object displacement and motion. This sensitivity is used in camera-based interferometers to measure nanometer-scale deformations between two camera exposures in a technique called electronic speckle pattern interferometry[1, 2]. Usually, this sensitivity to axial motion prevents the use of most interferometric techniques on moving objects. However, interferometric measurements on moving objects would have very interesting applications: Multiwavelength digital holography (MWDH) is already being used for industrial in-line inspection of non-reflective surfaces, and the throughput of those application is limited by handling speed[3, 4]. Being able to measure without stopping the object is highly desirable in this application.

Using spatial phase-shifting and multiple wavelengths simultaneously, the phase at the beat frequency – and from it, a height map of the surface – can be extracted from a single camera image[5]. This technique works even for moving objects, as long as the direction of motion is purely perpendicular to the direction of observation[6] or in a well-known direction at constant speed – even on rotating objects[6, 7]. Those experiments were performed at 1× magnification, and show that for perpendicular motion, the sensitivity to motion increases with increasing aperture size: The rays through the edge of the aperture cover lager angles to the optical axis, so they are least perpendicular to the sensitivity vector[8].

In this work, we extend that sensor principle to a 10× magnification, and an NA of 0.42. Since the illuminating light can be concentrated on a smaller area, higher intensities and shorter camera exposures make up for the disadvantages of the large NA, and measurements on non-reflective surfaces are demonstrated at considerable speeds.

in: Lehmann, P.; Osten, W.; Gonçalves Jr., A. A.; Society of Photo-Optical Instrumentation Engineers – SPIE:
Optical Measurement Systems for Industrial Inspection XII. Proc. SPIE 11782, Paper 117821P (2021); doi: 10.1117/12.2591936

2. INTERFEROMETRIC SETUP

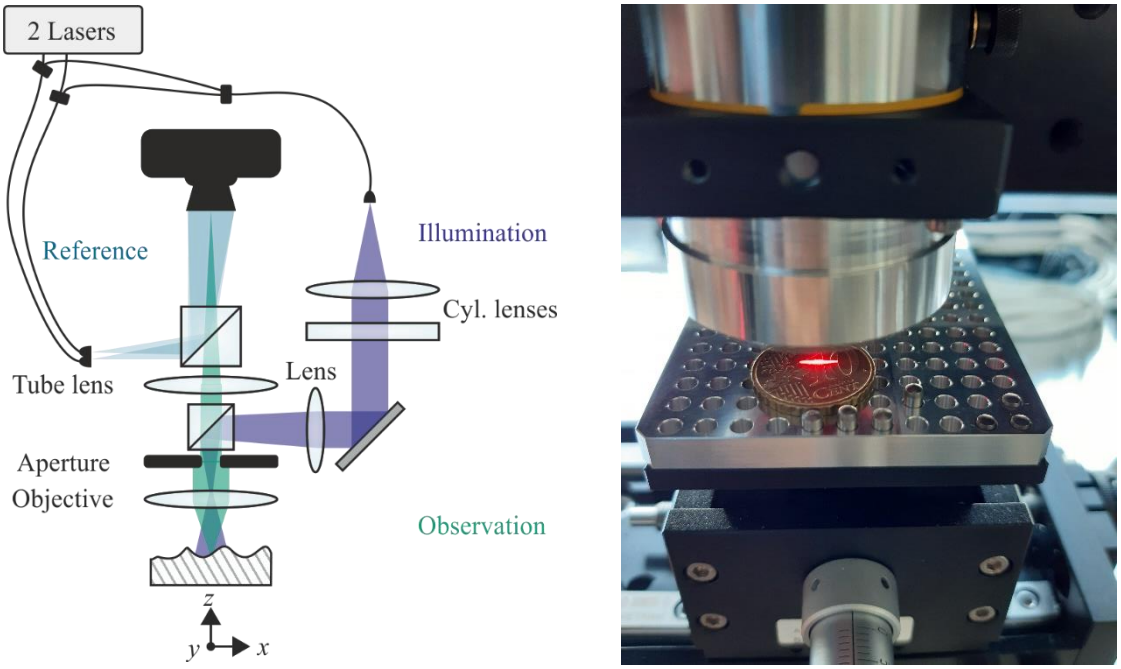

Figure 1: Left: Sketch of the interferometric setup. Right: Photograph of the coin underneath the 10× objective. The illuminated part of the coin is 3.7 × 0.2 mm² large – the raw image of this area is acquired simultaneously with both lasers in a single camera exposure.

The setup uses spatial phase-shifting, illuminating the object simultaneously with two continuous-wave lasers. The reference beams arrive at the camera at different angles to the observation axis, so that the differing spatial carrier frequencies are distinguishable and non-overlapping in Fourier space.

Figure 1 shows a sketch of the setup: two fiber-coupled lasers emit light at wavelengths of 637.76 nm and 632.87 nm. Each laser is split into illumination and reference beam by a fiber beam-splitter. A third beam-splitter combines the illumination waves. They are emitted from a common single-mode fiber into the sensor head. A pair of cylindrical lenses shapes the illumination beam into a line with an aspect ratio of about 20:1. A lens and a beam-splitter steer the illumination beam through the objective lens onto the object. In the object plane, the illumination beam is convergent, illuminating an area of about 3.7 × 0.2 mm². The total illumination power emitted from the objective is about 1.2 mW.

An objective (Mitutoyo M Plan Apo HR 10×, with tube lens MT-1, $f = 200$ mm) creates an in-focus image of the object on the camera (IOI Flare 48MP). A rectangular aperture (13.7 × 6.9 mm²) at the flange of the objective lens restricts the spatial frequencies transmitted through the imaging system, so that the diffraction patterns do not overlap in Fourier space (see section 3, Data Processing).

Two separate single-mode, polarization-maintaining fibers emit the reference beams, launching them at different angles through a combining beam-splitter onto the camera, where they create an interference pattern together with the observation beam. The camera acquires 10-bit images at 7920 × 512 px² per frame and 10 µs exposure time, transferring the data to a CoaxPress framegrabber.

To measure in motion, the interferometer is mounted upright above a linear motor (Micos UPM 150). The motor controller (SMC Hydra CM) generates trigger pulses at user-defined values of its integrated optical linear encoder. The leading edge of these pulses immediately trigger the camera, reducing jitter to sub-microsecond (and sub-micrometer) values. The images shown in the following were acquired at 35 mm/s, unless otherwise noted.

3. DATA PROCESSING

3.1 Single-image phase retrieval

A single camera frame captured by the setup shows only a small part of the object (Figure 2, top). Phase retrieval is performed using spatial phase shifting[9]: The reference beams at the two wavelengths are at different angles to the optical axis, resulting in different spatial carrier frequencies, visible in the fast Fourier transform of the image (Figure 2, bottom). Due to the rectangular aperture, these are limited in size to be non-overlapping, allowing easy separation.

Cropping the first diffraction orders and applying the inverse Fourier transform yields the complex-valued wavefront at individual wavelengths. Subtracting the visible-wavelength phases yields the phase at the synthetic wavelength of Λ_{syn} = 82.6 µm.

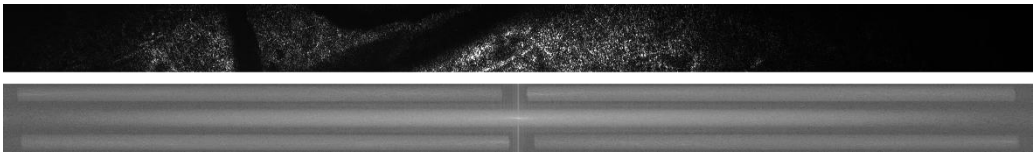

Figure 2: Top: raw camera image of a section of the coin in Figure 1. Bottom: FFT of the image, showing the distinct, non-overlapping diffraction orders in the four quadrants of the FFT.

3.2 Multi-image stitching

The complex-valued wavefronts of the 7920 × 512 px² regions are combined to a large image. In the overlapping regions, the complex sum is calculated. This corresponds to averaging the phase values while using amplitudes as weights, and improves data quality. During stitching, the data is resampled onto a grid with 2 µm pitch, yielding a stitched array of 1800×10000 px². This resampling is necessary because the motor translation between frames does not correspond to integer pixel steps. Decreasing the spatial sampling from the original 0.47 µm camera pixel pitch during this step avoids aliasing artifacts but does not significantly discard resolution, as the bandwidth of the objective was limited by the aperture and the high spatial frequencies were demodulated during single-image phase retrieval. The phase of the stitched result is shown in Figure 3, left.

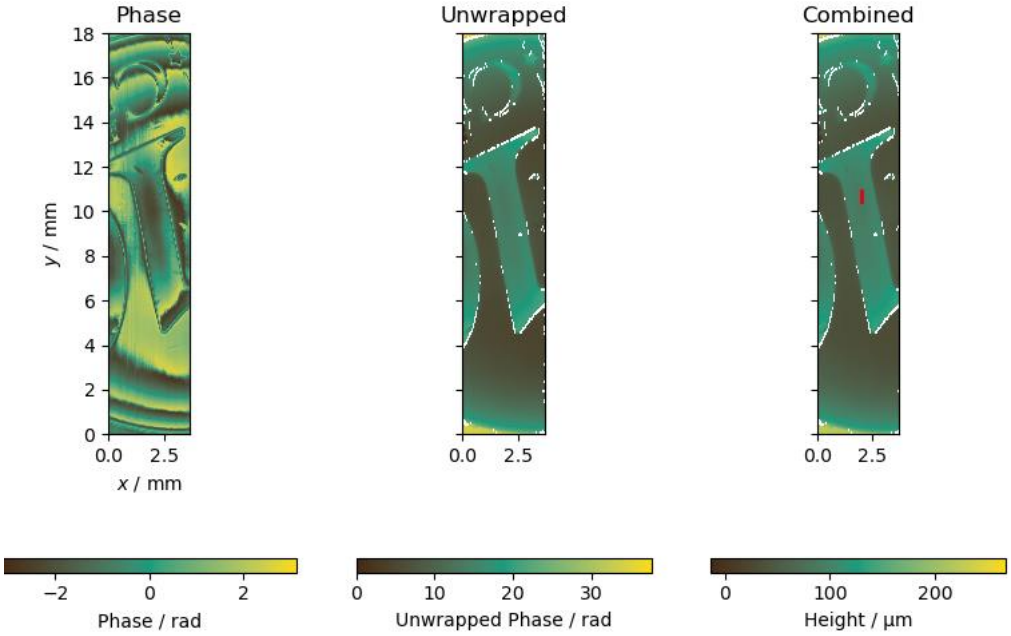

Figure 3: Measurements on a 10 Euro-Cent coin, acquired at 35 mm/s. Left: Stitched phase at synthetic wavelength, Center: Filtered and unwrapped phase. Right: unfiltered phase combined with unwrapped image, converted to height map of the object. Acquisition of this data took about 0.5 s.

The embossed “1” and a “C” are visible, but the height of the characters on the coin exceeds the unambiguous measurement range of 41.3 µm. Assuming a continuous surface, the phase jumps can be unwrapped. To speed up the unwrapping, an image downsampled by another factor of 4 is unwrapped. To retain the full axial and lateral resolution of the original phase map, the unwrapped image is upsampled and combined with the original phase image to a full-resolution, unambiguous image. This is similar to combining signals at different synthetic wavelengths[10]. The result is shown in Figure 3, right, converted to height units.

4. RESULTS

4.1 Stitching

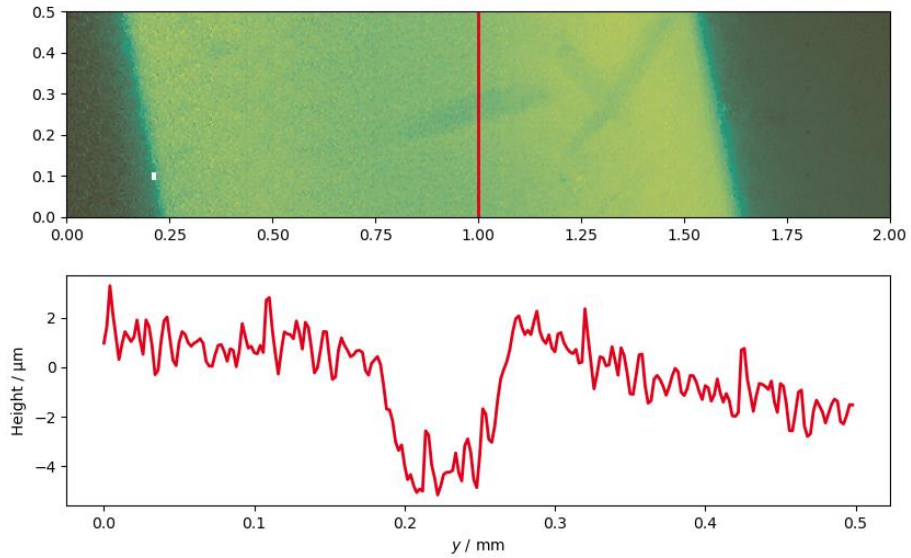

Figure 4: Top: Detail showing the area surrounding red line in Figure 3. At this magnification, scratches and dents in the coin are visible. Bottom: cross-section along the red line, showing that this dent is only about 5 µm deep.

The resolution of the microscopic setup is high enough that all phase jumps on the edges of the features in the phase map in Figure 3 can be resolved and the full area can be unwrapped. In a macroscopic setup, these edges would be too steep, and multiple phase jumps would occur within a single pixel, making unwrapping impossible. Even though it is downsampled, this image still has 1800 × 10000 px². In Figure 4, a small detail of the coin shows the resolution of the measurement: a small dent, less than 100 µm wide and only about 5 µm deep. The dent is very well resolved, showing the potential of this setup for inline defect detection and measurement.

4.2 Repeatability

To quantify the measurement quality, measurements on a groove normal (Halle KNT 2080/03) were performed and evaluated. The results are displayed in Tabe 1. The flat, nearly reflective surface is suitable for determining the local noise. The standard deviation of the height values in a flat 40 × 40 px² region is σ_{local}. It is 0.7 µm and 1.0 µm at 35 mm/s and 75 mm/s, respectively, corresponding to $\Lambda_{\mathrm{syn}}/118$ and $\Lambda_{\mathrm{syn}}/83$, respectively.

For absolute height measurements, the average value in such a region at the bottom of a groove is compared to regions on the top surface on the normal. To compensate tilt, the top is evaluated on two areas on opposite sides of the groove. This evaluation is repeated on a series of measurements – separate motion, triggering and acquisition of the images. The average height values and standard deviations σ_{height} are shown in Table 1.

Tabe 1: Local RMS noise σ_{local} and standard deviation σ_{height} of a step height measured on a groove normal.

Calibration	Measured, 35 mm/s			Measured, 75 mm/s		
Height / µm	σ_{local} / µm	Height / µm	σ_{height} / µm	σ_{local} / µm	Height / µm	σ_{height} / µm
7.502 ± 0.012	± 0.7	7.584	± 0.008	± 1.0	7.565	± 0.015
2.395 ± 0.010		2.491	± 0.008		2.425	± 0.013

The standard deviations σ_{height} are in the range of 10 nm, and are close to $\sigma_{height} = \sigma_{local} / N_{px}^{1/2}$, the value expected when averaging over N_{px} values with purely random errors. This indicates that the local deviations determined on flat areas of the sample is indeed random noise.

The absolute values of the height values differ from the calibration height – and, surprisingly, even between the measurements at different speeds – by several σ_{height}. This is most likely due to shifts in the laser wavelengths, which were not monitored with sufficient precision. For example, the measured values for the 2.4 µm groove differ by 2.6%: a wavelength shift of 120 pm in one of the lasers is sufficient to cause this difference. Such a shift is not unusual during the course of several hours for the stabilized laser diodes used for the experiment. For better absolute values in an inspection setting, the lasers would need to be monitored more closely. For highest precision, a wavelength meter could be synchronized to the camera and measure the wavelengths simultaneously to every single measurement.

It is noteworthy that the data were acquired at 35 mm/s – at this speed, the entire coin dataset takes only 0.5 s, so that even after stitching with overlap and downsampling, the measurement rate for the resulting height values shown in the figures is roughly 35 million/s. At 75 mm/s, the final data point rate is 75 million/s, accordingly.

5. CONCLUSION

By measuring in motion, the full bandwidth of modern cameras is utilized – in contrast to a motion system that has to fully stop for each frame of a stitched measurement, spending more time waiting for the motion system than acquiring data. This sensor delivers microscopic height maps with σ_{local} = 1 µm at 75 million points per second. This demonstrates that multi-wavelength digital holography using a microscope objective is a precise high-speed measurement technology ready for applications.

ACKNOWLEDGEMENT

Financial support by the German Federal Ministry of Education and Research (FKZ: 13N14009, "HoloMotion") is gratefully acknowledged.

REFERENCES

[1] Jacquot, P., “Speckle Interferometry. A Review of the Principal Methods in Use for Experimental Mechanics Applications,“ Strain 44(1), 57–69 (2008).

[2] Beckmann, T., Fratz, M., Bertz, A. and Carl, D., “High-speed deformation measurement using spatially phase-shifted speckle interferometry,“ SPIE Proceedings, 90060E (2014).

[3] Fratz, M., Beckmann, T., Schiller, A., Seyler, T., Bertz, A., Carl, D. and Buse, K., “Digital Holography: Evolution from a Research Topic to a Versatile Tool for the Inline 100% 3D Quality Control in Industry,“, 286–289 (2017).
[4] Fratz, M., Beckmann, T., Anders, J., Bertz, A., Bayer, M., Gießler, T., Nemeth, C. and Carl, D., “Inline application of digital holography [Invited],“ Appl. Opt. 58(34), G120 (2019).
[5] Takeda, M. and Yamamoto, H., “Fourier-transform speckle profilometry: three-dimensional shape measurements of diffuse objects with large height steps and/or spatially isolated surfaces,“ Applied Optics 33(34), 7829–7837 (1994).
[6] Schiller, A. F., Beckmann, T., Fratz, M., Belzer, D., Bertz, A., Carl, D. and Buse, K., “Multiwavelength Digital Holography with Spatial Phase Shifting on Moving Objects,“ OSA technical digest (online), DM3I.6 (2016).
[7] Schiller, A., Beckmann, T., Fratz, M., Bertz, A., Carl, D. and Buse, K., “Motion compensation for interferometric off-center measurements of rotating objects with varying radii,“ APL Photonics 4(7), 71301 (2019).
[8] Schiller, A., Beckmann, T., Fratz, M., Belzer, D., Bertz, A., Carl, D. and Buse, K., “Digital holography on moving objects: interference contrast as a function of velocity and aperture width,“ Applied Optics 56(16), 4622–4628 (2017).
[9] Ichioka, Y. and Inuiya, M., “Direct phase detecting system,“ Applied Optics 11(7), 1507–1514 (1972).
[10] Wagner, C., Osten, W. and Seebacher, S., “Direct shape measurement by digital wavefront reconstruction and multiwavelength contouring,“ Optical Engineering 39(1), 79–85 (2000).